Contemporary Fault Mechanics in Southern Alaska

James L. Kalbas, Andrew M. Freed, and Kenneth D. Ridgway

Department of Earth and Atmospheric Sciences, Purdue University, West Lafayette, Indiana, USA

Thin-shell finite-element models, constrained by a limited set of geologic slip rates, provide a tool for evaluating the organization of contemporary faulting in southeastern Alaska. The primary structural features considered in our analysis are the Denali, Duke River, Totschunda, Fairweather, Queen Charlotte, and Transition faults. The combination of fault configurations and rheological properties that best explains observed geologic slip rates predicts that the Fairweather and Totschunda faults are joined by an inferred southeast-trending strike-slip fault that crosses the St. Elias Mountains. From a regional perspective, this structure, which our models suggest slips at a rate of ~8 mm/a, transfers shear from the Queen Charlotte fault in southeastern Alaska and British Columbia northward to the Denali fault in central Alaska. This result supports previous hypotheses that the Fairweather–Totschunda connecting fault constitutes a newly established northward extension of the Queen Charlotte–Fairweather transform system and helps accommodate right-lateral motion (~49 mm/a) of the Pacific plate and Yakutat microplate relative to stable North America. Model results also imply that the Transition fault separating the Yakutat microplate from the Pacific plate is favorably oriented to accommodate significant thrusting (23 mm/a). Rapid dip-slip displacement on the Transition fault does not, however, draw shear off of the Queen Charlotte–Fairweather transform fault system. Our new modeling results suggest that the Totschunda fault, the proposed Fairweather–Totschunda connecting fault, and the Fairweather fault may represent the youngest stage of southwestward migration of the active strike-slip deformation front in the long-term evolution of this convergent margin.

1. INTRODUCTION

Active collisional and transpressional fault systems in southern and central Alaska are driven by oblique convergence between the Pacific and North American plates and collision of the Yakutat microplate [Figure 1; e.g., *Lahr and Plafker*, 1980; *Bruns*, 1983; *Bruhn et al.*, 2004; *Pavlis et al.*, 2004; *Matmon et al.*, 2006]. This convergent system has produced rapid uplift in coastal mountain ranges, large-magnitude earthquakes along the plate margin and within the overriding plate, and a broad zone of active deformation and seismicity that stretches for 500 km inboard of the Alaskan coast [*Plafker*, 1969; *Page et al.*, 1991; *Fletcher*, 2002; *Eberhart-Phillips et al.*, 2003; *Pavlis et al.*, 2004; *Bemis and Wallace*, 2007; *Lesh and Ridgway*, 2007]. Although the locations of faults in coastal and interior Alaska are fairly well established, their relative contemporary roles in accommodating oblique plate convergence are not well understood.
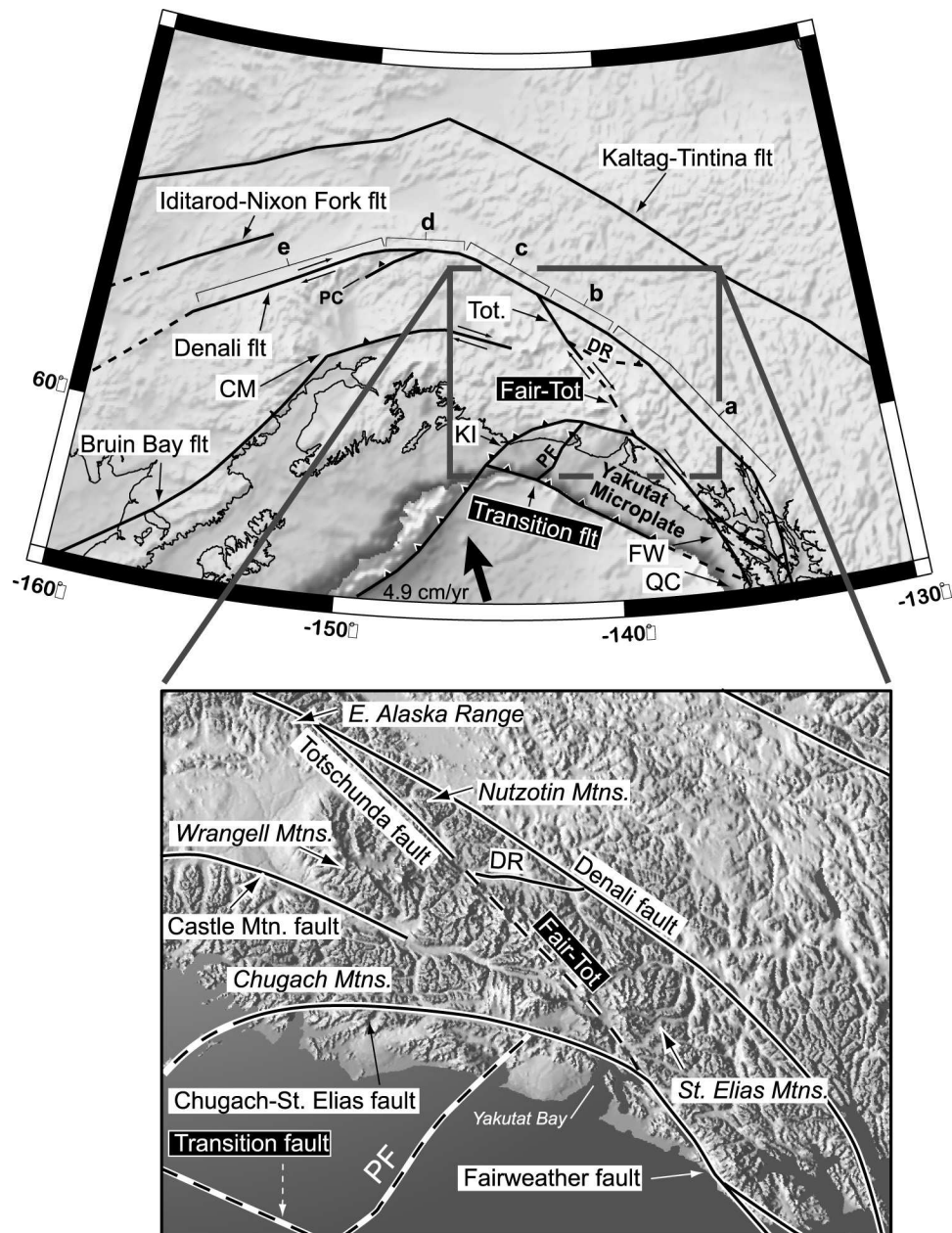
Figure 1. Shaded relief map of central and southern Alaska showing the location of major faults, including the proposed Fairweather–Totschunda connecting fault and the Transition fault, the two faults that our study focuses on (highlighted with white text and a black box). The Denali fault is subdivided into five segments (a–e) for the benefit of discussion in the text. Thick black arrow shows the motion of the Pacific plate relative to North America [*DeMets et al.*, 1994]. CM, Castle Mountain fault; DR, Duke River fault; FW, Fairweather fault; KI, Kayak Island; PC, Pass Creek fault; PF, Pamplona fault zone; QC, Queen Charlotte transform fault; Tot, Totschunda fault; Fair–Tot, Fairweather–Totschunda connecting fault. Inset, detailed view of the study region.

The primary constraint on long-term strain accumulation in the region comes from measurements of Quaternary geologic slip rates at locations along the Denali, Totschunda, Fairweather, and Castle Mountain faults (Table 1). Remote, mountainous terrane, and glacial cover, however, preclude a larger number of direct measurements along many parts of these fault systems. Consequently, displacement rates on most of the major faults are not well constrained (in several cases, it is not entirely clear whether certain segments are even active). As a result, the manner in which modern plate convergence is accommodated remains unclear. In this study, we use available geologic slip rates to constrain thin-shell finite-element models that test various candidate active fault configurations for contemporary southern Alaska. We specifically address two outstanding issues: (1) how shear strain transfers northward from the Queen Charlotte–Fairweather transform system inboard to the Denali fault system and (2) whether the Yakutat microplate moves as part of the Pacific plate or represents an independent block.

2. TECTONIC QUESTIONS

Differential motion across the northeastern Pacific plate margin is primarily taken up by the right-lateral strike-slip Queen Charlotte fault and its northern, mostly onshore counterpart, the Fairweather fault (Figure 1). At ~58°N, the Fairweather fault projects inboard of the Pacific coast and transitions into a series of roughly margin-parallel strike- and oblique-slip faults that form the boundaries of the Yakutat microplate [the Transition fault and the Chugach–St. Elias and Kayak island fault zones; Figure 1; *Plafker et al.*, 1978, 1994b; *Lahr and Plafker*, 1980; *Doser and Lomas*, 2000; *Bruhn et al.*, 2004]. Inboard of the Yakutat microplate, north–northwestward Pacific plate motion relative to North America produces oblique slip that is partitioned into contraction primarily at the plate margin (along the Aleutian megathrust) and strike-slip deformation along the inland Denali, Totschunda, and Castle Mountain faults (Figure 1).

Table 1. Geologic and Modeled Estimates of Slip Rates on Select Faults in Southern Alaska[a]

Fault (segment)	Slip Rate, mm/a	Motion Sense	Reference
Geologic observations			
Fairweather fault	40	Strike-slip (RL)	*Page* [1969]
Fairweather fault	46 ± 9.5	Strike-slip (RL)	*Plafker et al.* [1978]
Denali fault (segment a)	1.0 ± 2.0	Strike-slip (RL)	*Plafker et al.* [1994a]
Denali fault (segment a)	0	Strike-slip (RL)	*Richter and Matson* [1971]
Denali fault (segment b)	8.4 ± 2.2	Strike-slip (RL)	*Matmon et al.* [2006]
Denali fault (segment c)	12.1 ± 1.7	Strike-slip (RL)	*Matmon et al.* [2006]
Denali fault (segment c)	10.7 10.9	Strike-slip (RL)	*Plafker et al.* [2006]
Denali fault (segment d)	9.4 ± 1.6	Strike-slip (RL)	*Matmon et al.* [2006]
Totschunda fault (northern)	10 20	Strike-slip (RL)	*Plafker et al.* [1977]
Totschunda fault (northern)	11.5	Strike-slip (RL)	*Plafker et al.* [1994a]
Totschunda fault (northern)	6.0 ± 1.2	Strike-slip (RL)	*Matmon et al.* [2006]
Castle Mt. fault	<1 2.7	Transpression (RL)	*Haeussler et al.* [2000, 2002]
Chugach–St. Elias fault	<30	Oblique slip	*Bruhn et al.* [2004]
Broxon Gulch fault	1.4	Reverse	*Stout and Chase* [1980]
Model estimations			
Fairweather fault	41 ± 3 to 51 ± 4	Strike-slip (RL)	*Lisowski et al.* [1987]
Fairweather fault	34.7 41.0	Strike-slip (RL)	*Fletcher* [2002]
Fairweather fault	45.6 ± 2.0	Strike-slip (RL)	*Fletcher and Freymueller* [2003]
Denali fault (segment a)	3.8 ± 1.4	Strike-slip (RL)	*Fletcher and Freymueller* [2003]
Denali fault (segment c)	9	Strike-slip (RL)	*Fletcher* [2002]
Castle Mt. fault	5	Strike-slip (RL)	*Fletcher* [2002]
Transition fault	21 ± 3	Reverse-oblique	*Fletcher* [2002] and *Fletcher and Freymueller* [2003]
Transition fault	10 30	Reverse-oblique	*Pavlis et al.* [2004]
Queen Charlotte transform	48	Strike-slip (RL)	*Nishenko and Jacob* [1990]

[a] Denali fault segments are shown in Figure 1.

Although the major contemporary faults in southern Alaska have been identified, the level of activity of individual fault segments and their role in partitioning strain remain poorly understood. One of the primary questions in Alaskan neotectonics is how strain is distributed between the Pacific plate boundary and strike-slip faults in the North American interior. Several workers have speculated on the basis of geomorphic features identified in aerial photographs that the Totschunda fault projects southeastward through the glacier-mantled St. Elias Mountains, forming a modern strike-slip boundary that transfers slip between the Fairweather and central Denali faults [*St. Amand*, 1957; *Grantz*, 1966; *Hamilton and Meyers*, 1966; *Page*, 1969; *Richter and Matson*, 1971; *Naugler and Wageman*, 1973; *Plafker et al.*, 1978; *Fletcher*, 2002]. This idea was partially supported by the 2002 $M = 7.9$ Denali earthquake, which demonstrated active slip along the Totschunda fault, as opposed to the eastern Denali fault [*Eberhart-Phillips et al.*, 2003; *Bhat et al.*, 2004]. An unequivocal link between the Fairweather and Totschunda faults, however, has not been confirmed by geologic or geophysical studies and may be impossible to confirm while the area is covered with ice. Slip associated with the 2002 Denali earthquake, for example, did not project into the St. Elias Mountains. Broad-scale mapping of lithological contacts has constrained total offset on part of the proposed Fairweather–Totschunda connecting fault (near Hubbard Glacier) to no more than ~0.5 km [*Plafker et al.*, 1978]. In contrast, offset geologic markers along-strike to the south, along the Artlewis fault (a northwest-trending splay off the Fairweather fault that projects beneath the St. Elias ice fields), demonstrate 16 ± 5 km of cumulative right-lateral slip (probably since ~35 Ma; G. Plafker, written communication 2007). The relative roles of the Totschunda fault, the proposed Fairweather–Totschunda connecting fault, and eastern segments of the Denali fault in accommodating long-term regional deformation remain unclear.

Using kinematic block models, *Lahr and Plafker* [1980] demonstrated that the proposed Fairweather–Totschunda connecting fault is in a favorable position to accommodate strain. In addition, southeastern extensions of the Denali fault (the Lynn Canal and Chatham Strait segments of *Wright and Wright* [1908], *St. Amand* [1957], and *Plafker et al.* [1978]) appear to slip slowly (<2 mm/a) or not at all. The model of *Lahr and Plafker* [1980] adequately reproduced the range of slip rates observed and inferred at the time for the Fairweather and eastern Denali faults but may have overpredicted the slip rate of the Totschunda fault (10 mm/a of calculated right-lateral slip versus the 6.0 ± 1.2 mm/a of slip observed by *Matmon et al.* [2006]). The discrepancy in slip-rate estimations reflects an overestimation by *Lahr and Plafker* [1980] of the northward velocity of the Pacific plate as it was inferred at the time (63 mm/a), their simplifying assumption of blocklike deformation throughout the model domain, and their assumption of a latest Wisconsinan (10 ka) age for offset morainal deposits [*Lahr and Plafker*, 1980]. The purely kinematic model also did not account for deformation along the eastern Denali fault north of 60°N. Although slip-rate estimations by *Matmon et al.* [2006] remain to be validated by subsequent studies, their data show that the eastern Denali fault slips at a rate of 8.4 ± 2.2 mm/a immediately east of the Totschunda fault intersection, apparently drawing some shear strain away from the Totschunda fault.

Another possibility is that neither the Denali fault nor the Totschunda fault connects to the Queen Charlotte–Fairweather transform system, with contemporary shear instead being accommodated by distributed anelastic deformation and reverse slip along contractional structures [*Bird*, 1996]. Using a thin-shell numerical code, *Bird* [1996] calculated relatively low rates of anelastic shear strain (5×10^{-16} s^{-1}) in the form of distributed contractional deformation southwest of the southeastern Denali fault. The Fairweather–Totschunda connecting fault was not considered in Bird's model. Rather, contractional deformation north of the Yakutat microplate produced elevated continuum shear strain rates (2×10^{-14} s^{-1}). This model also produced rapid reverse slip along the Duke River fault, a possible splay of the eastern Denali fault system (Figure 1).

Along with uncertainty about levels of fault activity, the magnitude of differential motion between the Pacific plate and the Yakutat microplate is unclear. The Yakutat microplate primarily consists of continental and transitional oceanic crustal fragments (the Yakutat terrane of *Plafker et al*. [1994b]; Figure 1) that were excised in mid-Cenozoic time from the western margin of North America. Emplacement of the Yakutat microplate is the latest in a series of accretionary events to occur in southern Alaska and one of the few examples of such collisions currently active anywhere in the world. Thus, determining whether the Yakutat microplate is coupled to the northward-moving Pacific plate or behaves as a separate entity will enhance our understanding of the regional tectonics of southern Alaska and will provide insight into a long-standing model for processes of continental accretion. Several geodetic, geologic, seismological, and modeling studies have calculated reverse to oblique motion across the Transition fault that separates the Yakutat microplate from the Pacific plate, although the range of inferred slip rates is quite large [4–24 mm/a; *Lahr and Plafker*, 1980; *Perez and Jacob*, 1980; *Page et al.*, 1989; *Fletcher*, 2002; *Pavlis et al.*, 2004]. *Lahr and Plafker* [1980], for example, used a low convergence rate (4 mm/a) across the trailing edge of the microplate to generate their kinematic model of south-

ern and central Alaska. In contrast, *Fletcher and Freymueller* [1999] and *Freymueller et al*. [this volume] used GPS measurements to calculate a velocity for the Yakutat microplate relative to the Pacific plate of 21 mm/a; this motion is presumably accommodated across the Transition fault. One argument against a rapid convergence between the Pacific plate and Yakutat microplate, however, is the apparent lack of deformation in ~800 m of sediment that overlie the Transition fault escarpment [*Bruns*, 1979; *Lahr and Plafker*, 1980; *Pavlis et al.*, 2004; *Gulick et al.*, 2007]. This argument becomes less important if these sediments are too young to have accumulated significant deformation [*Pavlis et al.*, 2004].

3. OBSERVATIONAL CONSTRAINTS

Slip rate estimates from various geologic indicators provide the best constraints on long-term (10^3–10^6 a) fault activity. Table 1 shows inferred slip rates for major faults in central and southern Alaska. The Queen Charlotte fault and its northern counterpart, the Fairweather fault, are thought to accommodate much of the estimated 49.1 ± 1.4 mm/a of northward Pacific plate motion relative to North America [Figure 1; e.g., *Lahr and Plafker*, 1980; *Niskenko and Jacob*, 1990; *DeMets et al.*, 1994]. *Plafker et al.* [1978] estimated between 48 and 58 mm of average annual slip on the Fairweather fault during Holocene time based on their measurements of offset drainages near the offshore–onshore transition zone southeast of Yakutat Bay (Figure 1, inset). Errors associated with moraine ages, however, allow for as little as 36.6 mm/a of right-lateral slip [*Plafker et al.*, 1978]. Previously published slip-rate estimates for the Fairweather fault based on elastic screw dislocation models are comparatively low. *Lisowski et al.* [1987] estimated between 41 ± 3 and 51 ± 4 mm/a of slip, whereas least-squares inversion of geodetic observations provides a best-fit slip rate of 45.6 ± 2.0 mm/a, assuming a locking depth of 9.0 ± 0.8 km [*Fletcher and Freymueller*, 2003].

Slip rates on the Denali, Totschunda, and Castle Mountain faults also provide primary model constraints. Numerous measurements allow us to subdivide the Denali fault into an eastern strand (segment a in Figure 1), central strands (segments b and c), and western strands (segments d and e). Average slip rates vary along strike from little or no contemporary motion along the easternmost segment (a) to as much as 12.1 ± 1.7 mm/a of right-lateral slip along the central segment west of the Totschunda intersection (segment c) and 9.4 ± 1.6 mm/a of slip along western fault exposures [segment d; Table 1; *Plafker et al.*, 1994a, 2006; *Matmon et al.*, 2006]. The Totschunda fault extends southeastward from the central Denali fault and lies along strike with an unproven structural boundary, referred to here as the Fairweather–Totschunda

connecting fault, that is thought to project southward through the St. Elias Mountains (Figure 1, inset). *Plafker et al.* [1977, 1994a] reported relatively rapid slip rates (10–20 mm/a) for the Totschunda fault based on offset geomorphic features assumed to be of Wisconsinan age; *Matmon et al.* [2006] revise the estimation of Pleistocene–Holocene slip to 6.0 ± 1.2 mm/a. Reliable slip-rate estimates are not available for the proposed Fairweather–Totschunda connecting fault in the St. Elias Mountains [*Plafker et al.*, 1978]. Mapping [*Plafker et al.*, 1978], however, constrains right-lateral displacement on the Totschunda fault segment near Hubbard Glacier to 0.5 km. Based on a slip rate of 6 mm/a [*Matmon et al.*, 2006], the fault should not be much more than ~80,000 years old. In contrast to the low cumulative displacements recorded along the Totschunda fault, however, ~16 km of right-lateral displacement occurred along the Artlewis fault, a probable southerly segment of the proposed Fairweather–Totschunda connection fault (G. Plafker, written communication). This high cumulative displacement allows activity along the fault to have initiated as early as 2.7 Ma ago, although the age of these offsets are unknown. Approximate rates of right-lateral transpression along the Castle Mountain fault based on balanced cross sections were provided by *Haeussler et al.* [2000; <1–3 mm/a of probable Pleistocene slip].

4. ANALYSIS APPROACH

The analysis objective is to find the combination of fault configurations and rheological properties that best explains observed geologic slip rates in central and southern Alaska. We use the finite-element code SHELLS [*Kong and Bird*, 1995] to approximate lithospheric deformation over a spherical model domain with laterally varying thickness and strength characteristics. SHELLS is used to solve for time-averaged velocities and strain rates across numerous earthquake cycles. This approach cannot consider the effects of elastic strain accumulation associated with locked faults or postseismic relaxation processes following large earthquakes. Thus, geodetic observations are not appropriate constraints for the present models, especially in southern Alaska, which is still experiencing postseismic effects associated with the 1964 $M = 9.2$ Alaska earthquake. An advantage of the shell modeling approach is that relatively short computation times enable analysis of the influence of changes in assumed fault configuration and rheological strength on fault-slip rates for a large number of configurations and model parameters.

Two previous finite-element studies, *Lundgren et al.* [1995] and *Bird* [1996], addressed modes of regional deformation in southern Alaska. *Lundgren et al.* [1995], using fault-slip rates and weighted very long baseline interferometry

rates to constrain models for crustal deformation in south-
ern and central Alaska, produced fault-slip patterns that
generally agree with geologic observations. Their models,
however, used a simplified microplate configuration for the
southern margin (i.e., the Yakutat block and Pacific plate
are coupled across the Transition fault) and did not include
a Totschunda–Fairweather connecting fault. Our modeling
approach is similar to that of *Bird* [1996], who conducted
a plate-scale dynamic study of deformation in Alaska us-
ing the thin-shell finite-element code, PLATES. Bird, how-
ever, assumed a specific fault configuration (that did not
include the Fairweather–Totschunda connecting fault) and
a viscoelastic strength distribution and solved for the coef-
ficients of fault and continuum friction that most closely ex-
plained observational constraints. In contrast, we solve for
the best-fitting fault configuration and associated rheological
strength. Simulations using PLATES also relied on a Carte-
sian coordinate system to produce a flat-Earth mesh, thereby
introducing local errors into regional-scale model solutions
[*Kong and Bird*, 1995]. The present study uses a spheri-
cal thin-shell mesh with an improved elemental resolution
(Figure 2).

4.1. Model Domain and Boundary Conditions

The model domain used in this study includes the bulk
of the northwestern North American plate and the northern-
most Pacific plate (Figure 2). Model boundaries include a
fixed eastern margin that stretches northward along the sta-
ble North American craton to the pole and a western bound-
ary that coincides with the approximate western margin of
the North American plate. Compression along the western
plate margin in Kamchatka and Siberia is approximated us-
ing boundary thrust faults; deformation along the Nansen
Ridge, the northwestern mesh boundary, is similarly mod-
eled using extensional fault nodes. Bounding fault nodes are
assigned velocities based on the NUVEL-1A plate model
[*DeMets et al.*, 1994].

We include a section of the Pacific plate along the entire
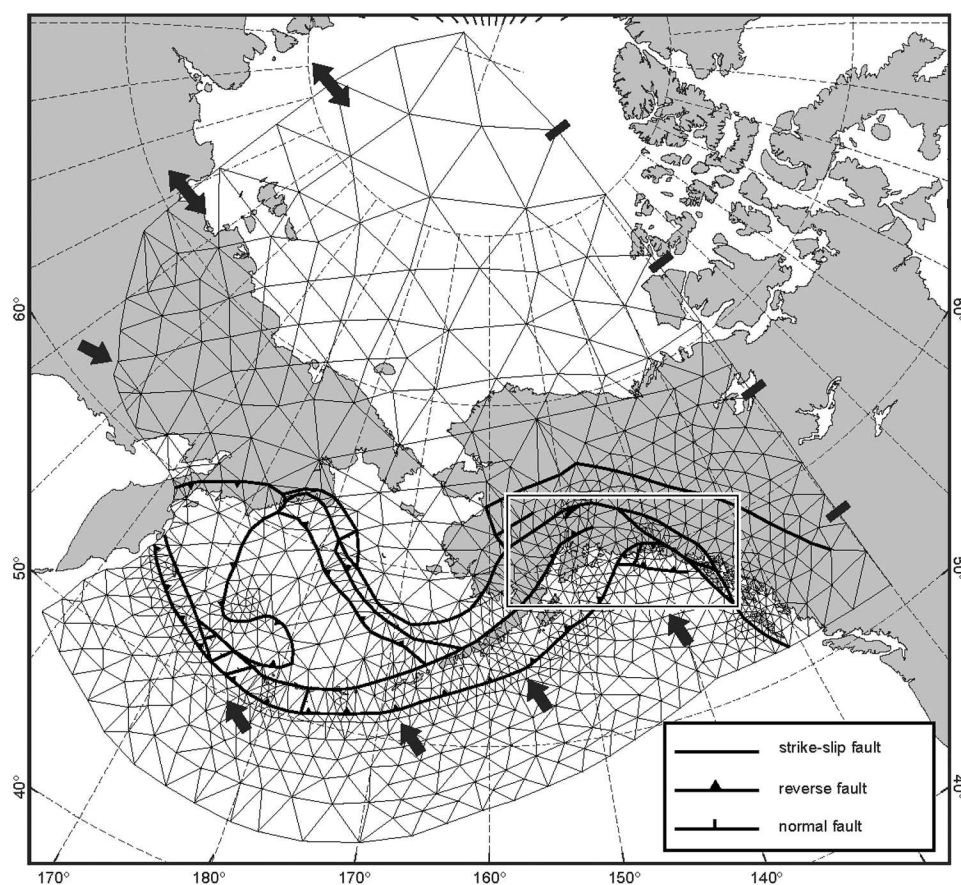length of the Aleutian trench and approximate the lubricating

Figure 2. Finite-element grid used for numerical experiments. Box shows the area enlarged in Figure 4.

effect of water-laden subducted sediment along the Aleutian megathrust by automatically limiting the downdip integral of shear traction to 2.5 10^{12} N/m [e.g., *Bird*, 1978; *Kong and Bird*, 1995]. Velocities derived from the NUVEL-1A plate model [*DeMets et al.*, 1994] were assigned to boundary nodes within the Pacific plate. We approximate active fault geometries in the Bering Sea region from *Worrall* [1991] and adopt the assumption of *Bird* [1996] of westward-extending Denali and Bruin Bay faults in the Bering Sea region.

4.2. Lithospheric Structure

Topography is considered in the modeling as a source of vertical stress associated with an assumption of Airy isostasy, although the 2-D finite-element grid is a smooth spherical thin shell (r = 6371 km). Heat flow is used to determine crustal thickness and to calculate lateral rheological strength variations that are based on an integration of vertical transitions from Coulomb friction in the upper crust and dislocation creep in the lower crust and mantle (constitutive relationships are adopted from *Kong and Bird* [1995] and *Bird* [1996]). We vary the continuum strength envelope in experimental runs by changing assumptions of continuum friction (values range from f_c = 0.5–1.0) and viscoelastic strength. Figure 3 shows several rheologies considered in our analysis including that of a weak lower crust with a strong mantle, that of a strong lower crust with a weak mantle, and cases where the crust and mantle are both strong and weak. Laboratory flow laws considered for each case are listed in Table 2. While a variety of flow laws for the crust and mantle are available, we choose four that are sufficient to explore the influence of relative strength associated with each layer. The distribution of heat flow is based on the compilation of *Blackwell and Richards* [2004], although modifications in heat flow are used to explore the influence of rheological strength on fault-slip rates.

Faults in the brittle portion of the modeled crust are given variable dips based on geologic observations. All strike-slip faults are approximated as vertical structures, whereas reverse faults are modeled with a 30° dip and normal faults with a 60° dip (Figure 2). Trench segments were modeled using a uniform 20° dip, which, in SHELLS space, allows for a reduced downdip integral of shear traction. Fault strength is determined by an assumed coefficient of friction, f_f, which is restricted to be common for all faults. We consider a range from f_f = 0.05 to f_f = 0.30 in our numerical experiments.

4.3. Model Evaluation

Each candidate model (fault configuration and rheology) leads to predictions of slip style (reverse, normal, or strike-slip), slip rate, and azimuth that can be compared
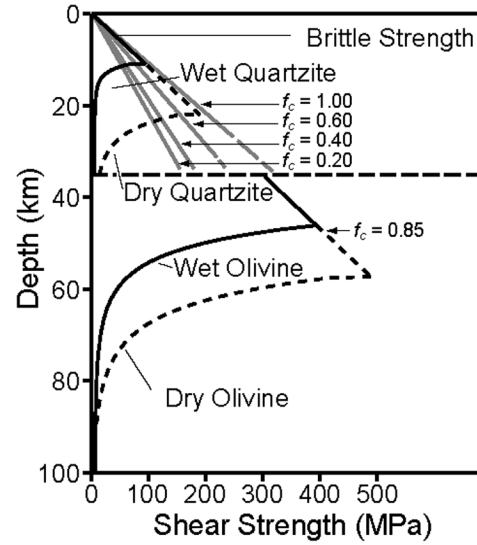

Figure 3. Strength envelopes for the lithosphere considered in this study. Solid lines show the rheology of the best-fit model. Dashed and gray lines show alternative viscoelastic and continuum friction (f_c) rheologies considered, respectively. In the calculations, strength of the lithosphere is based on a vertical integration of the envelopes shown here (see text).

with observed quantities (Table 1). Weighted ^{2} misfits are calculated based on the rate and direction of slip relative to observed values based on the relationship:

$$\chi^2 = \frac{1}{N} \sum_{r,a=1}^{N} \left(\frac{[r_i^o - r_i^c]^2}{\sigma_{r_i}^2} + \frac{[a_i^o - a_i^c]^2}{\sigma_{a_i}^2} \right), \qquad (1)$$

where N is the number of fault locations compared, r_i^0 and a_i^0 are the measured slip rate and slip direction (degrees from north) of individual faults, r_i^c and a_i^c are the calculated slip rate and slip direction of individual fault nodes, and $_{r_i}$ and $_{a_i}$ are the errors of measured slip rate and slip azimuth data (Table 1).

5. RESULTS

5.1. Best-Fit Model

Observed geologic slip rates are best explained by a finite-element mesh that includes a Fairweather–Totschunda

Table 2. Intensive Parameters for all Models

Intensive parameters (crust/lithospheric mantle)				
Mean density	2816/3332 kg m^{-3}			
Thermal expansion coefficient	$2.4 \times 10^{-5}/3.1 \times 10^{-5}$ K^{-1}			
Thermal conductivity	3.0/4.06 m^{-1} K^{-2}			
Radioactive heat production	$4.55 \times 10^{-7}/3.2 \times 10^{-8}$ W m^{-3}			
Friction coefficient, continuum	Best fit = 0.85			
Friction coefficient, faults	Best fit = 0.17			

Description and mineralogy	A, MPa^{-n} s^{-1}	n	Q, kJ/mol	Reference
Best-fit viscoelastic rheology				
Weak crust (wet quartzite)	2.9×10^{-3}	1.8	151	*Jaoul et al.* [1984]
Weak mantle (wet olivine)	4.89×10^{6}	3.5	515	*Hirth and Kohlstedt* [1996]
Alternate viscoelastic rheologies				
Strong crust (dry quartzite)	3.4×10^{-6}	2.8	184	*Jaoul et al.* [1984]
Strong mantle (dry olivine)	4.89×10^{4}	3.5	535	*Hirth and Kohlstedt* [1996]

connecting fault and a strength distribution that includes a wet quartzite crust and wet olivine mantle (with $f_c = 0.85$ and $f_f = 0.17$). This fault configuration and strength distribution leads to the minimum misfit with respect to the range of observed fault-slip rates (case 1 in Table 3). Figure 4a shows that predicted strike-slip motion along the eastern Pacific plate margin decreases northward from 42 mm/a in the south to 39 mm/a on the Fairweather fault east of the Yakutat microplate and 36 mm/a at the Fairweather–Totschunda connecting fault intersection. Adjacent to this intersection, right-lateral transpression is locally taken up by the Chugach–St. Elias fault (the best-fit model predicts a contraction rate of ~22 mm/a on the fault). The predicted rate of transpressional motion along the northern boundary of the Yakutat microplate is consistent with deformation rates documented by *Bruhn et al.* [2004], although we were forced to simplify their "contact" fault and the Chugach–St. Elias fold-and-thrust belt into a single boundary (Figure 1; refer also to Section 6 for a discussion of the implications of this simplification). A component of thrust motion across the Yakutat foreland also agrees with observations of coseismic shoreline uplift in the Yakutat Bay region following the 1899 earthquake sequence [*Thatcher and Plafker*, this volume]. Modeled slip rates along the Fairweather–Totschunda connecting fault demonstrate partitioning of strain northwestward away from the Fairweather–Chugach–St. Elias fault system. The best-fit model predicts ~10 mm/a of right-lateral slip directly adjacent to the fault intersection with the Fairweather fault [i.e., along the Artlewis fault segment according to G. Plakfer, written communication), diminishing northwestward from to 8 mm/a at 62°N latitude and 6 mm/a along the Totschunda fault segment near the intersection with the Denali fault (Figure 4a).

The best-fit model suggests that along with accommodating significant right-lateral displacement (6–8 mm/a) through the St. Elias and Wrangell Mountains, the Totschunda and Fairweather–Totschunda connecting faults transmit shear strain from the plate margin northward to the central Denali fault (segments c and d in Figure 1; Figures 4a and 4b). Nodal velocity estimations, for example, show a continuum of north- to northwest-trending vectors southwest of the Fairweather–Totschunda connecting fault from the Chugach–St. Elias fault to central Denali fault segments that have markedly different orientations and magnitudes than their counterparts to the immediate northwest (Figure 4b). The best-fit fault configuration produces modeled slip rates that are consistent with observed deformation rates for the central Denali fault. Calculated slip rates vary along the strike of the Denali fault from 7 mm/a on segment b to 11 mm/a on segment c and 9 mm/a on segment d. Comparable slip rates between the northern Totschunda fault segment and the Denali fault immediately east of the Totschunda intersection suggest that strain is evenly distributed between these subparallel fault systems in south-central Alaska.

Models also suggest that the larger-scale, long-term strain budgets of the southeastern and northwestern Denali and Fairweather–Totschunda connecting fault systems are also equivalent. The sum of the modeled long-term slip rate for the southern part of the Fairweather–Totschunda connecting fault (i.e., the Artlewis fault segment of G. Plafker, written communication; 8–10 mm/a) and the southeastern segment of the Denali fault (3 mm/a) is approximately equal to the sum of the long-term rates observed near the Denali fault–Totschunda fault intersection point (6 mm/a on Totschunda fault and 7 mm/a on the Denali fault east of the intersection point), thereby suggesting equivalent partitioning of slip

Table 3. Results of Finite-Element Experiments Showing Calculated Fault-Slip Rates of Individual Structures and Resulting χ^2 Misfits[a]

Model	Figure	Segment d 9.4 ± 1.6	Segment c 12.1 ± 1.7	Segment b 8.4 ± 2.2	Fair onshore 46 ± 8.5	Totschunda 6.0 ± 1.2	Castle Mt. 2.2 ± 1.8	FW-2 offshore	Fair–Tot connect	Segment e	Segment a	Trans. fault	χ^2 value fault slip
1 Best-fit model ($f_f = 0.17; f_c = 0.85$)	Figure 4a	**8.9**	**11.0**	**7.0**	**39.7**	**5.8**	**1.3**	42.0	7.9	4.5	2.6	23.0	**0.56**
2 No Fair–Tot connecting fault	Figure 4c	**7.8**	9.6	**9.9**	**39.0**	0.9	**1.0**	42.0	–	4.1	3.5	26.0	**2.25**
3 No SE Denali fault	Figure 4d	**8.5**	10.0	**6.2**	**39.0**	**6.1**	**1.2**	41.0	8.3	4.2	–	24.0	**0.70**
4 Partial SE Denali fault	–	**8.6**	**11.0**	**6.8**	**40.0**	**5.7**	**1.2**	40.0	7.8	4.3	2.6	24.0	**0.60**
5 Trans fault connects to FW	Figure 4e	3.5	4.3	1.7	11.0	3.5	0.0	44.0	4.7	2.3	1.0	44.0	**2.52**
6 High-traction Trans fault	–	17.0	21.0	**8.6**	**38.0**	16.0	**1.6**	41.0	17.0	6.4	2.1	6.9	**3.49**
7 Low-traction Chugach fault	–	4.7	6.2	**6.2**	**40.0**	1.4	0.0	43.0	4.1	2.9	1.8	1.3	**1.98**
8 Alt fault friction ($f_f = 0.30$)	–	**10.0**	**12.0**	**9.7**	31.0	4.0	5.0	40.0	5.5	5.0	3.6	8.8	**0.84**
9 Alt fault friction ($f_f = 0.14$)	–	**8.8**	10.0	**6.6**	**42.0**	**5.6**	**1.1**	42.0	7.8	4.8	2.3	22.0	**0.70**
10 Alt fault friction ($f_f = 0.11$)	–	**8.4**	9.8	**6.2**	**45.0**	**5.2**	**0.9**	42.0	7.4	4.8	2.1	22.0	**0.71**
11 Alt fault friction ($f_f = 0.08$)	–	7.6	8.8	5.6	**48.0**	4.6	**0.8**	43.0	6.9	4.7	1.3	22.0	**1.00**
12 Alt fault friction ($f_f = 0.05$)	–	6.4	7.2	4.6	**51.0**	3.8	**0.6**	44.0	5.9	4.2	1.2	23.0	**1.43**
13 Alt continuum friction ($f_c = 0.60$)	–	**9.3**	**11.0**	**7.3**	**39.0**	**6.1**	**1.4**	41.0	8.3	4.8	2.8	23.0	**0.56**
14 Alt continuum friction ($f_c = 0.40$)	–	**9.5**	**11.0**	**7.8**	**37.0**	**5.7**	**1.6**	40.0	7.7	5.1	3.1	24.0	**0.59**
15 Alt continuum friction ($f_c = 0.20$)	–	6.9	8.4	**6.9**	**27.0**	2.9	**1.4**	36.0	4.3	4.1	2.8	33.0	**1.42**

[a] Bold text emphasizes calculated values that are within the error range of measured geologic slip rates. Alt, alternative; Fair-Tot, Fairweather-Totschunda; Trans, Transition fault; SE, St. Elias fault.
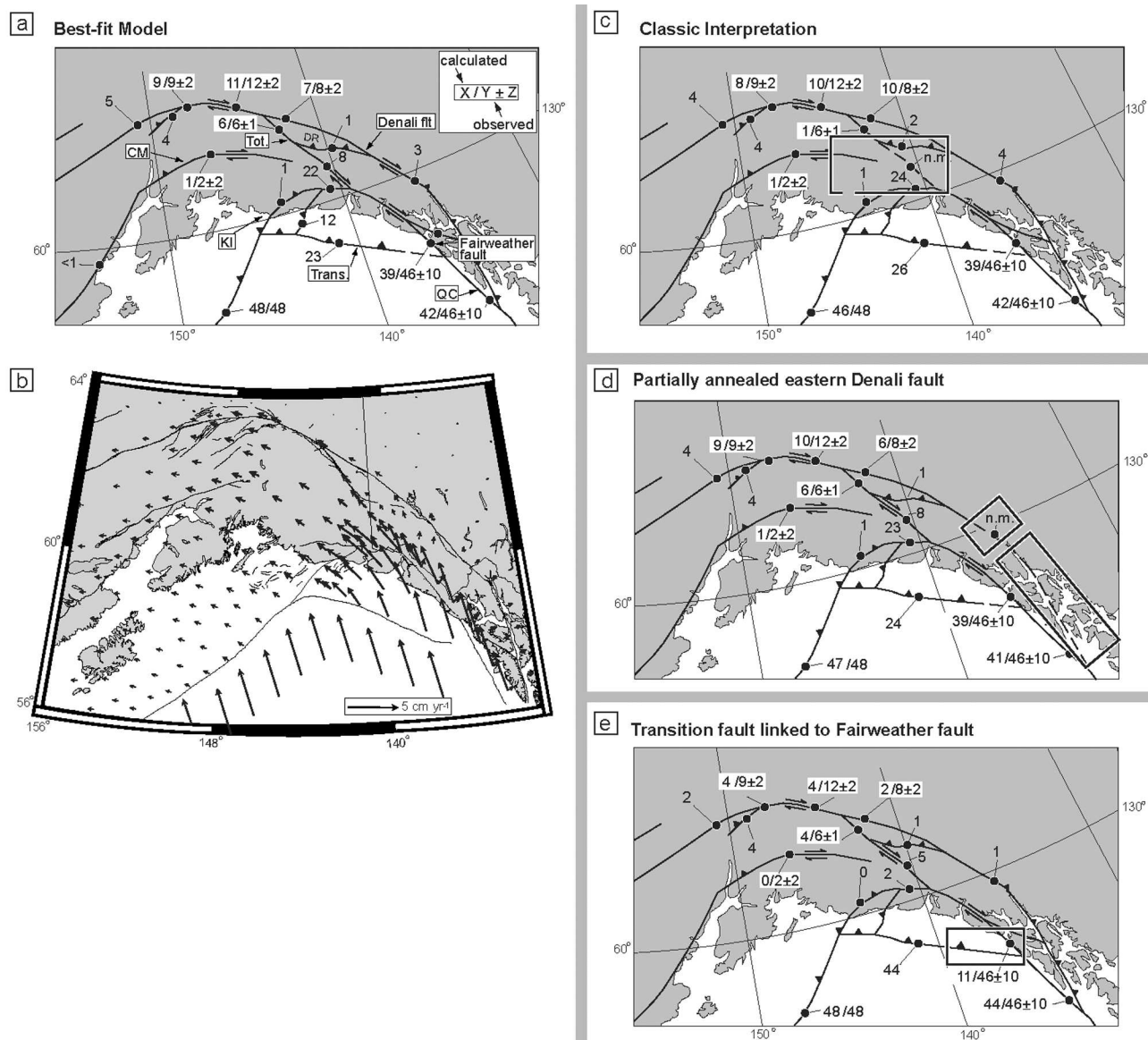
Figure 4. Comparison of calculated and observed fault-slip rates for several candidate fault configurations. Modeled interior faults outside the region shown here slip at rates between 0 and 1 mm/a; the Queen Charlotte fault south of Chatham Strait slips at a rate of 48 mm/a. (a) Fault-slip rates for the best-fit model (minimum misfit to observed slip rates, see Table 3) with a through-going Fairweather–Totschunda connecting fault. CM, Castle Mountain fault; DR, Duke River fault; KI, Kayak Island fault; QC, Queen Charlotte transform; Tot., Totschunda fault; Trans., Transition fault. (b–g) Alternative fault configurations considered (see highlighted black in white box in each panel) that led to greater misfit to observed slip rates. (b) Nodal velocities relative to stable North America for the best-fit model. Note the diminishing magnitude of northwest-directed velocity vectors across the Fairweather–Totschunda connecting fault. (c) The classic interpretation of fault geometries in southern Alaska excludes the Fairweather–Totschunda connecting fault. The fault is dashed here to show that it is excluded from the mesh. (d) Alternative fault configuration in which the eastern Denali fault (dashed line) is prevented from slipping. (e) Alternative fault configuration in which the Transition fault projects eastward to the Fairweather fault.

between the two systems. In the Totschunda fault region, the Duke River fault accounts for ~1 mm/a of contractional deformation between the eastern Denali and Totschunda faults, consistent with the observations of *Gedney* [1970], *Power* [1988], and *Page et al.* [1991] on seismicity. Although the timing of initial contractional deformation adjacent to the Duke River fault is not known, thrust faults truncate 10-Ma-old lavas [*Campbell and Dodds*, 1982a, 1982b, 1982c, 1982d). This model solution also predicts 1 mm/a of right-lateral oblique slip on the Castle Mountain fault that degrades westward to <1 mm/a of reverse motion (Figure 4a), consistent with observations by *Haeussler et al.* [2000, 2002].

By fitting known deformation rates in southern Alaska, slip rates on faults without geologic constraints can be inferred from the best-fit model solution. For example, the best-fit model predicts that the southeastern and western segments of the Denali fault (segments a and e in Figure 1) accommodate relatively minor right-lateral slip (3 and 5 mm/a, respectively). In contrast to the model of *Lundgren et al.* [1995], which predicted a component of left-lateral motion along faults in southern southwestern Alaska when using NUVEL-1a Aleutian convergence rates, our model predicts purely right-lateral motion on faults west of the central Alaskan syntaxis, consistent with geologic observations. The best-fit model also predicts that the Transition fault accommodates rapid dip-slip (23 mm/a) but does not draw shear away from the Fairweather fault, else high modeled slip rates to the north would greatly diminish. The robustness of these requirements is discussed in more detail in the following sections.

The continuity of shear accommodation along the Queen Charlotte, Fairweather, Totschunda, and Denali fault systems and the Fairweather–Totschunda connecting fault implies blocklike motion in southern Alaska. The model, however, predicts a level of distributed shear locally within the continuum lithosphere. The main regions of distributed deformation are in the vicinity of the St. Elias Mountains and the central Alaska Range, both of which are predicted to accommodate shear strain rates (1.4×10^{-15} to 3.0×10^{-15} s^{-1}) that are an order-of-magnitude higher than the surrounding regions (10^{-16} to 10^{-17} s^{-1}). Although calculated strain rates cannot be easily compared directly with inferred uplift rates using a shell model, these regions of high continuum deformation coincide with large, rapidly uplifted and/or uplifting mountains [e.g., *Fitzgerald et al.*, 1995; *Sheaf et al.*, 2003].

5.2. Alternatives to a Fairweather–Totschunda Connecting Fault

The requirement of slip along a strike-slip boundary between the Fairweather and Totschunda faults, as opposed to

distributed anelastic deformation, becomes apparent when the fault is removed. Figure 4c (case 2 in Table 3) shows that this configuration produces only 1 mm/a of calculated slip on the Totschunda fault to the north, well below the 6.0 ± 1.2 mm/a of slip inferred by *Matmon et al.* [2006]. Calculated slip rates on the central Denali fault (segment c) also fall below the error range of Holocene geologic constraints when the Fairweather–Totschunda connecting fault is removed from the model domain. East of the intersection between the Totschunda and Denali faults, the latter slips too rapidly (10 mm/a compared with the observed 8 mm/a), as this section accommodates shear strain no longer taken up by the Fairweather–Totschunda connecting fault.

If the Fairweather–Totschunda connecting fault plays a significant role in transferring shear stress from the Queen Charlotte–Fairweather transform system to the central Denali fault, it raises the question of whether the eastern Denali fault remains an integral part of the regional fault-slip budget. If the southeastern portion of the Denali fault is locked, the rate of slip on the Denali fault to the north (immediately east of the Totschunda fault intersection) decreases only by 1 mm/a (Figure 4d; case 3 in Table 3). This is perhaps surprising since the southeastern Denali segment was inferred to slip <4 mm/a in the best-fit model. Similarly, extending the southeastern Denali fault southward to 60°N produces no significant change in regional strain accommodation (case 4 in Table 3). These model results imply that the eastern Denali fault may no longer play a vital role in the neotectonics of southeastern Alaska and that the Totschunda fault has become or is in the process of becoming the principal means of strain accommodation inboard of the Fairweather fault.

5.3. Alternative Transition Fault Configurations

The best-fit numerical model requires that the Transition fault along the trailing edge of the Yakutat microplate (1) does not redirect strain away from the Queen Charlotte–Fairweather transform fault system and (2) accommodates the bulk of contractional deformation produced by Pacific plate convergence, with relatively minor amounts of reverse slip occurring along the Chugach–St. Elias and Kayak Island faults. In the best-fit model, the Transition fault does not redirect shear from the Fairweather fault because it does not extend far enough eastward to make contact. If, however, we allow the Transition fault to extend eastward and form a triple junction with the Fairweather fault, we find that this new model greatly underpredicts the rate of slip on the Fairweather fault to the north (11 mm/a versus an observed minimum of ~37 mm/a, Figure 4e; case 5 in Table 3). In this configuration, shear is accommodated by rapid reverse

motion (44 mm/a) across the Transition fault. Not surprisingly, less shear is transferred from the Fairweather fault inboard to interior faults and westward through the syntaxis along the northern margin of the Yakutat microplate (Figure 4e). With a modeled triple junction, predicted slip rates on all interior faults fall well below observed values, and the right-lateral slip rate on the Chugach–St. Elias fault decreases from the best-fit solution by 90% (Table 3).

To test the requirement of high strain accommodation along the trailing margin of the Yakutat microplate, we ran an alternative model where high shear tractions limit significant strain accommodation along the Transition fault (case 6 in Table 3). As expected, strengthening the Transition fault results in a reduced reverse slip rate (6.9 mm/a from the best-fit model rate of 23.0 mm/a). However, it also produces anomalously high slip rates on the Totschunda fault (16 mm/a compared with 6 mm/a observed) and the central (21 compared with 12 mm/a observed) and western (17 compared with 9 mm/a observed) segments of the Denali fault. An alternative to imparting lower shear traction on the Transition fault is to prescribe lower shear tractions on the Chugach–St. Elias and Kayak Island faults (case 7 in Table 3). This configuration, however, leads to greatly reduced right-lateral slip rates on interior structures. For example, central and western segments of the Denali fault slip between 5 and 6 mm/a, well below observed values of –912 mm/a, and the Totschunda fault slips at just 1 mm/a compared with the observed rate of 6 mm/a.

5.4. Alternative Coefficients of Fault Friction and Alternative Rheologies

Varying the coefficient of friction on faults alters the way in which strain associated with subduction is partitioned throughout our models of southern Alaska. Higher friction (e.g., $f_f \geq 0.3$) reduces the rate of slip on the Aleutian megathrust, therefore transferring a greater load inboard. This increased load is accommodated by inboard faults, which slip more rapidly despite an increased coefficient of fault friction here as well (case 8 in Table 3). Slip on the Castle Mountain fault, for example, increases to 6 mm/a, well above the inferred 2-mm/a rate, when a friction of 0.3 is assumed for all faults. Similarly, reductions in the coefficient of fault friction below the best-fit value of 0.17 result in rapid slip along the Aleutian megathrust and diminished slip rates of inland faults below observed values (cases 9–12 in Table 3).

Models are less sensitive to changes in the brittle failure envelope for the continuum lithosphere. Incremental reductions in the frictional strength of continuum elements result in only small decreases in the slip rates of interior faults (Figure 3; Cases 13–15 in Table 3), presumably a response to greater strain accommodation within the continuum lithosphere. A low internal friction coefficient ($f_c = 0.20$ compared with the best-fit value, $f_c = 0.85$), for example, reduces the slip rate of the central Denali fault by 27% and the Totschunda fault by 50% while increasing the absolute strain rate of the continuum lithosphere in vicinity of the eastern Yakutat microplate.

The wet quartzite (weak) lower crust and wet olivine (weak) mantle used in the best-fit model is, in part, consistent with regional studies of lithospheric strength in southern Alaska. A wet olivine mantle is consistent with the rheology inferred from postseismic deformation following the 2002 Denali earthquake [*Freed et al.*, 2006]. While this postseismic analysis inferred a relatively strong crust, models reflected a short, 3-year postseismic time interval. It is possible that over the long term, as simulated by this analysis, the lower crust has time to flow and behaves in a weak manner.

We also considered three alternative flow laws (Table 2). Central segments of the Denali fault are sensitive to changes in the modeled rheology, whereas most other faults maintain slip rates that are consistent with the best-fit model. A flow law consistent with wet quartzite crust and dry olivine mantle reduces slip rates on Denali fault segments b and c by 3 and 2 mm/a, respectively. As strength at any one element is based on an integration of the strength envelope, assuming a dry crust/wet mantle rheology produces a similar degradation of slip rates as the wet crust/dry mantle rheology. The onshore Fairweather fault-slip rate (39 mm/a) in both dry crust/wet mantle and wet crust/dry mantle cases remains in the range of measured uncertainty (46 ± 10 mm/a) but decreases from the best-fit rate of 42 mm/a. These alternative flow laws also produce slight increases in the slip rate of the Fairweather–Totschunda connecting fault (9 mm/a versus the best-fit rate of 8 mm/a). The decrease in calculated slip rates along the Denali fault in response to increased lithospheric strength occurs with a simultaneous increase in calculated slip rates along the Aleutian megathrust. This result implies that a greater proportion of shear strain may be accommodated at the plate boundary, therefore imparting less stress to inboard faults. For example, assuming an even stronger strength profile, a dry crust/dry mantle rheology, produces significantly diminished slip rates for central and western segments of the Denali fault in conjunction with systematically increased modeled slip rates for the Aleutian megathrust.

6. DISCUSSION

An intriguing possibility for the longer-term fault-displacement budget in southeastern Alaska based on our

new modeling results and previous geologic studies is that regional strike-slip displacement has stepped progressively southwestward throughout Cenozoic time. The geologic evidence for this interpretation is compelling at a regional scale, but locally incomplete. The earliest direct evidence for strike-slip displacement on major faults in southeastern Alaska comes from syntectonic sedimentary strata that fill several fault-adjacent pull-apart basins [e.g., *Ridgway*, 1992; *Ridgway and DeCelles*, 1993a, 1993b]. Because pull-apart basin development is a function of fault displacement [*Crowell*, 1974a, 1974b; *Aydin and Nur*, 1982], documentation of the age of syntectonic strata along major fault systems provides ages for strike-slip displacement [*Ridgway et al.*, 1999; *Trop et al.*, 2004]. For example, Cenozoic pull-apart basins along the eastern Denali fault system (Figure 1) are uncommon, and attempts to date the few strata exposed along the fault system have not been successful [*Ridgway et al.*, 1995]. Correlation of offset Jurassic–Lower Cretaceous strata, however, requires ~350 km of right-lateral displacement [*Eisbacher*, 1976; *Nokleberg et al.*, 1985; *Lowey*, 1998] on this segment of the Denali fault system, but there is little direct evidence for Cenozoic displacement. In addition, seismicity studies have recorded few earthquakes along this segment of the fault system, suggesting that the easternmost part of the Denali fault system is relatively inactive [*Page et al.*, 1991].

In contrast, the next major fault to the southwest, the Duke River fault (Figure 1), has a well-developed Upper Eocene–Lower Oligocene stratigraphic record in fault-adjacent pull-apart basins [*Ridgway et al.*, 1995, 2002]. The Duke River fault has also offset the lower part of the Miocene Wrangell Lavas; ^{40}Ar/^{39}Ar ages of truncated lavas have ages of 17.8 and 16.0 Ma [*Ridgway et al.*, 1992]. Geologic studies have documented lavas with ^{40}Ar/^{39}Ar ages of 11.0 and 10.4 Ma that overlie the Duke River fault [*Ridgway et al.*, 1992]; these lavas mark the end of regional strike-slip displacement along this part of the fault system. Seismicity studies show that the Duke River fault is characterized by active north–south compression [*Gedney*, 1970; *Power*, 1988]. The earthquake data are consistent with regional folds and local thrust faults that have been well documented in mapping studies of the Wrangell Lavas adjacent to the Duke River fault [*Campbell and Dodds*, 1982a, 1982b, 1982c, 1982d]. The end of both volcanism and strike-slip displacement at 10 Ma along the Duke River fault [*Skulski et al.*, 1991, 1992] has been interpreted to represent the incipient collision of continental crust of the Yakutat terrane with the southern margin of southcentral Alaska [*Ridgway et al.*, 1992; *Trop and Ridgway*, 2007].

The next major fault system to the southwest is the Totschunda fault (Figure 1). Our new modeling results suggest that the Totschunda fault, the proposed Fairweather–Totschunda connecting fault, and the Fairweather fault may represent the youngest stage of southwestward migration of the active strike-slip deformational front in the long-term evolution of this convergent margin. The Totschunda fault is interpreted to be a Holocene structure [*Richter and Matson*, 1971; *Plafker et al.*, 1977]. As discussed earlier, from a kinematic perspective, it appears that the Totschunda fault is or may be connecting with the active Fairweather fault system along the northern margin of the Yakutat block (including the northwestward Artlewis fault splay; G. Plafker, written communication 2007). Unfortunately, our methods, directed at understanding regional trends, limit the elemental resolution with which we are able to model the northern boundary of the Yakutat block (without unreasonably deforming individual triangular elements). The onshore component of the Pamplona deformation zone, for example, bends sharply eastward near the Malaspina Glacier, then trends for some 150 km subparallel to the boundary fault and structures that comprise the Yakutat foreland. Recognizing the complexity of contractional structures along that margin, we included a single, freely slipping thrust fault (labeled PF in Figure 1), which mimics the trend of the active deformation front of the Pamplona Zone and part of the contractional foreland [e.g., *Bruhn et al.*, 2004; *Pavlis et al.*, 2004]. Although our best-fit model predicts significant thrust motion (~12 mm/a) for this simplified Pamplona structure, the cumulative effects of contractional deformation on a number of subsidiary en echelon faults in the Yakutat foreland may well influence the net amount of slip attributed here to the Fairweather–Totschunda connecting fault. Future work might consider resolving regional-scale faults or approximating brittle foreland behavior with a weak anelastic near-surface rheology. Northwestward transfer of strike-slip motion from Fairweather fault to the Fairweather–Totschunda connecting fault, however, appears from our results to be compatible with rapid contractional foreland deformation along the northern margin of the Yakutat block.

The cause of the proposed southwestward shift in strike-slip displacement is probably closely linked with the ongoing collision of the Yakutat microplate [e.g., *Plafker*, 1987; *Bruhn et al.*, 2004; *Pavlis et al.*, 2004] as well as transition from a strike-slip- to a subduction-dominated margin along the southern coast of Alaska [*Doser and Lomas*, 2000]. At a first approximation, the space problem caused by the collision of the Yakutat microplate may have required the strike-slip deformational front to have stepped progressively southwestward to maintain a regional strike-slip fault orientation conducive for transport of crustal material through the syntaxis represented by this tight corner in southcentral Alaska.

7. CONCLUSIONS

The neotectonic framework of southeastern Alaska is still only partly understood due to its remote setting and steep, highly glaciated topography. In this type of setting, thin-shell finite-element models provide a useful tool for discriminating between contrasting fault geometries and lithospheric strength profiles. To evaluate the organization of contemporary faulting in southern Alaska, we tested our models against known geologic slip rates at a number of locations. The best-fit model uses a relatively weak lower crust and upper mantle rheology and requires a continuum of strike-slip deformation between the Totschunda and Fairweather faults located in the St. Elias Mountains. We refer to this inferred zone of deformation as the Fairweather–Totschunda connecting fault; this fault slips at a predicted rate of 8 mm/a in our best-fit model. As noted by previous authors, minimal offset (~0.5 km) of units require the Fairweather–Totschunda connecting fault to be a recently established strike-slip boundary. Results suggest that the Fairweather, Totschunda, and Fairweather–Totschunda connecting faults, along with central segments of the Denali fault, are the principle means of strain accommodation in southern Alaska. The eastern Denali fault, in contrast, is calculated to have a comparatively low rate of slip (<3 mm/a) and thus may no longer play a significant role in strain accommodation. The model results along with available geologic data from faults in southeastern Alaska and the western Yukon Territory suggest that the strike-slip deformation front in southeastern Alaska may have stepped progressively southwestward to maintain a regional fault orientation conducive for transport of crustal material through the syntaxis. The best-fit model also suggests that the Transition fault at the trailing edge of the Yakutat microplate slips at a rate of 23 mm/a and, therefore, that the Yakutat microplate and the Pacific plate are not moving as a single entity. Slip rates on the Transition fault must diminish to the east, as the model indicates that shear strain accommodated by the Fairweather fault is not being bled off by the Transition fault.

REFERENCES

Aydin, A., and A. Nur (1982), Evolution of pull-apart basins and their scale independence, *Tectonics,* 1, 91–105.

Bemis, S. P., and W. K. Wallace (2007), Neotectonic framework of the north-central Alaska Range foothills, in *Tectonic Growth of a Collisional Continental Margin: Crustal Evolution of Southern Alaska*, edited by K. D. Ridgway, J. M. Trop, J. M. G. Glen, and J. M. O'Neil, *Geol. Soc. Am. Spec. Pap.*, p. 549–572.

Bhat, H. S., R. Dmowska, J. R. Rice, and N. Kame (2004), Dynamic slip transfer from the Denali to Totschunda faults, Alaska: Testing theory for fault branching, *Bull. Seismol. Soc. Am., 94*, S202–S213.

Bird, P. (1978), Stress and temperature in subduction shear zones: Tonga and Mariana, *Geophys. J. R. Astron. Soc., 55*, 411–434.

Bird, P. (1996), Computer simulations of Alaskan neotectonics, *Tectonics, 15*, 225–236.

Blackwell, D. D., and M. Richards (2004), Calibration of the AAPG Geothermal Survey of North America BHT Data Base, Poster session paper 87616, AAPG Annual Meeting, Dallas, Tex.

Bruhn, R. L., T. L. Pavlis, G. Plafker, and L. Serpa (2004), Deformation during terrane accretion in the Saint Elias orogen, Alaska, *Geol. Soc. Am. Bull., 116*, 771–787.

Bruns, T. R. (1979), Late Cenozoic structure of the continental margin, northern Gulf of Alaska, in *Proceedings of the 6th Alaska Geological Symposium,* edited by A. Sisson, pp. 11–130, Alaska Geological Society, Anchorage.

Bruns, T. R. (1983), Model for the origin of the Yakutat block, an accreted terrane in the northern Gulf of Alaska, *Geology, 11*, 718–721.

Campbell, R. B., and C. J. Dodds (1982a), Geology of the southwest Kluane Lake map area, Yukon Territory, *Geol. Surv. Can. Open File*, *829*.

Campbell, R. B., and C. J. Dodds (1982b), Geology of the southwest Dezadeash map area, Yukon Territory, *Geol. Surv. Can. Open File*, *831*.

Campbell, R. B., and C. J. Dodds (1982c), Geology of the Mount St. Elias map area, Yukon Territory, *Geol. Surv. Can. Open File*, *830*.

Campbell, R. B., and C. J. Dodds (1982d), Geology of the Tatshenshini River map area, British Columbia, *Geol. Surv. Can. Open File*, *926*.

Crowell, J. C. (1974a), Sedimentation along the San Andreas fault, California, in *Modern and Ancient Geosynclinal Sedimentation*, edited by R. H. Dott Jr. and R. H. Shaver, *Spec. Publ. Soc. Econ. Paleontol. Mineral., 19*, 292–303.

Crowell, J. C. (1974b), Origin of Late Cenozoic basins in southern California, in *Tectonics and Sedimentation*, edited by W. R. Dickinson, *Spec. Publ. Soc. Econ. Paleontol. Mineral., 22*, 190–204.

DeMets, C., R. G. Gordon, D. F. Argus, and S. Stein (1994), Effects of recent revisions to the geomagnetic reversal time scale on estimates of current plate motion, *Geophys. Res. Lett., 21*, 2191–2194.

Doser, D. I., and R. Lomas (2000), The transition from strike-slip to oblique subduction in southeastern Alaska from seismological studies, *Tectonophysics, 316*, 45–65.

Eberhart-Phillips, D., et al. (2003), The 2002 Denali fault earthquake, Alaska: A large magnitude, slip-partitioning event, *Science, 300*, 1113–1118.

Eisbacher, G. H. (1976), Sedimentology of the Dezadeash flysch and its implications for strike-slip faulting along the Denali fault, Yukon Territory and Alaska, *Can. J. Earth Sci., 13*, 1495–1513.

Fitzgerald, P. G., R. B. Sorkhabi, T. F. Redfield, and E. Stump (1995), Uplift and denudation of the central Alaska Range: A case study in the use of apatite fission track thermochronology to determine absolute uplift parameters, *J. Geophys. Res., 100*, 20,175–20,191.

Fletcher, H. J. (2002), Tectonics of interior Alaska from GPS measurements, Ph.D. dissertation, Univ. of Alaska, Fairbanks.

Fletcher, H. J., and J. T. Freymueller (1999), New GPS constraints on the motion of the Yakutat Block, *Geophys. Res. Lett., 26*, 3029–3032.

Fletcher, H. J., and J. T. Freymueller (2003), New constraints on the motion of the Fairweather fault, Alaska, from GPS observations, *Geophys. Res. Lett., 30*(3), 1139, doi:10.1029/2002GL016476.

Freed, A. M., R. Bürgmann, E. Calais, and J. Freymueller (2006), Stress-dependent power-law flow in the upper mantle following the 2002 Denali, Alaska, earthquake, *Earth Planet. Sci. Lett., 252*, 481–489.

Gedney, L. (1970), Tectonic stresses in southern Alaska in relationship to regional seismicity and the new global tectonics, *Bull. Seismol. Soc. Am., 60*, 1789–1802.

Grantz, A. (1966), Strike-slip faults in Alaska, *U.S. Geol. Surv. Open File Rep.*, 82 p.

Gulick, S. P. S., L. A. Lowe, T. L. Pavlis, J. V. Gardner, and L. A. Mayer (2007), Geophysical insights into the Transition fault debate: Propagating strike slip in response to stalling Yakutat block subduction in the Gulf of Alaska, *Geology, 35*, 763–766, doi:10.1130/G23585A.1.

Haeussler, P. J., R. L. Bruhn, and T. L. Pratt (2000), Potential seismic hazards and tectonics of the Upper Cook Inlet basin, Alaska, based on analysis of Pliocene and younger deformation, *Geol. Soc. Am. Bull., 112*, 1414–1429.

Haeussler, P. J., T. C. Best, and C. F. Waythomas (2002), Paleoseismicity at high latitudes: Seismic disturbance of upper Quaternary deposits along the Castle Mountain fault near Houston, Alaska, *Geol. Soc. Am. Bull., 114*, 1296–1310.

Hamilton, W., and W. B. Myers (1966), Cenozoic tectonics of the western United States, *Rev. Geophys., 4*, 509–549.

Hirth, G., and D. L. Kohlstedt (1996), Water in the oceanic upper mantle: Implications for rheology, melt extraction, and the evolution of the lithosphere, *Earth Planet. Sci. Lett., 144*, 93–108.

Jaoul, O., J. Tullis, and A. Kronenberg (1984), The effect of varying water contents on the creep behavior of Heavitree quartzite, *J. Geophys. Res., 89*, 4297–4312.

Kong, X., and P. Bird (1995), SHELLS: A thin-shell program for modeling neotectonics of regional or global lithosphere with faults, *J. Geophys. Res., 100*, 22,129–22,131.

Lahr, J. C., and G. Plafker (1980), Holocene Pacific–North American plate interaction in southern Alaska: Implications for the Yakataga seismic gap, *Geology, 8*, 483–486.

Lesh, M. E., and K. D. Ridgway (2007), Geomorphic evidence of active transpressional deformation in the Tanana foreland basin, south-central Alaska, in *Tectonic Growth of a Collisional Continental Margin: Crustal Evolution of Southern Alaska*, edited by K. D. Ridgway, J. M. Trop, J. M. G. Glen, and J. M. O'Neil, *Geol. Soc. Am. Spec. Pap. 431*, in press.

Lisowski, M., J. C. Savage, and R. O. Burford (1987), Strain accumulation across the Fairweather and Totschunda faults, Alaska, *J. Geophys. Res., 92*, 11,552–11,560.

Lowey, G. W. (1998), A new estimate of the amount of displacement on the Denali fault system based on the occurrence of carbonate megaboulders in the Dezadeash Formation (Jura-Cretaceous), Yukon, and the Nutzotin Mountains sequence (Jura-Cretaceous), Alaska, *Bull. Can. Petrol. Geol., 46*, 379–386.

Lundgren, P., F. Saucier, R. Palmer, and M. Langon (1995), Alaska crustal deformation: Finite element modeling constrained by geologic and very long baseline interferometry data, *J. Geophys. Res., 100*(B11), 22,033–22,045.

Matmon, A., D. P. Schwartz, P. J. Haeussler, R. Finkel, J. J. Lienkaemper, H. D. Stenner, and T. E. Dawson (2006), Denali fault slip rates and Holocene–late Pleistocene kinematics of central Alaska, *Geology, 34*, 645–648.

Naugler, F. P., and J. M. Wageman (1973), Gulf of Alaska: Magnetic anomalies, fracture zones, and plate interaction, *Geol. Soc. Am. Bull., 84*, 1575–1584.

Nishenko, S. P., and K. H. Jacob (1990), Seismic potential of the Queen Charlotte–Alaska–Aleutian seismic zone, *J. Geophys. Res., 95*, 2511–2532.

Nokleberg, W. J., D. L. Jones, and N. J. Silberling (1985), Origin and tectonic evolution of the Maclaren and Wrangellia terranes, eastern Alaska Range, Alaska, *Geol. Soc. Am. Bull., 96*, 1251–1270.

Page, R. A. (1969), Late Cenozoic movement on the Fairweather fault in southeastern Alaska, *Geol. Soc. Am. Bull., 80*, 1873–1878.

Page, R. A., C. D. Stephens, and J. C. Lahr (1989), Seismicity of the Wrangell and Aleutian Wadati–Benioff zones and the North American plate along the Trans-Alaska Crustal Transect, Chugach Mountains and Copper River basin, southern Alaska, *J. Geophys. Res., 94*, 16,059–16,082.

Page, R. A., N. N. Biswas, J. C. Lahr, and H. Pulpan (1991), Seismicity of continental Alaska, in *Neotectonics of North America*, edited by D. B. Slemmons, E. R. Engdahl, M. D. Zoback, and D. D. Blackwell, *Decade Map, 1*, 47–68, Geol. Soc. Am., Boulder, Colo.

Pavlis, T. L., C. Picornell, L. Serpa, R. L. Bruhn, and G. Plafker (2004), Tectonic processes during oblique collision: Insights from the St. Elias orogen, North American Cordillera, *Tectonics, 23*, TC3001, doi:10.1029/2003TC001557.

Perez, O. J., and K. H. Jacob (1980), Tectonic model and seismic potential of the eastern Gulf of Alaska and Yakataga seismic gap, *J. Geophys. Res., 85*, 7132–7150.

Plafker, G. (1969), Tectonics of the March 27, 1964, Alaska earthquake, *U.S. Geol. Surv. Prof. Pap.*, 543–1, 74 pp.

Plafker, G. (1987), Regional geology and petroleum potential of the northern Gulf of Alaska continental margin: Circum–Pacific Council for Energy and Mineral Resources, *Earth Sci. Ser., 6*, 229–268.

Plafker, G., T. Hudson, and M. Rubin (1977), Preliminary observations of late Cenozoic displacements along the Totschunda and Denali fault systems, *U.S. Geol. Surv. Circ.*, *733*, 67–69.

Plafker, G., T. Hudson, T. Burns, and M. Rubin (1978), Late Quaternary offsets along the Fairweather fault and crustal plate interactions in southern Alaska, *Can. J. Earth Sci., 15*, 805–816.

Plafker, G., L. M. Gilpin, and J. C. Lahr (1994a), Neotectonic map of Alaska, in *The Geology of Alaska*, edited by G. Plafker and H. C. Berg, *The Geology of North America, G-1*, Geol. Soc. of Am., Boulder, Colo., 1 sheet, scale 1:2,500,000.

Plafker, G., J. C. Moore, and G. R. Winkler (1994b), Geology of the southern Alaska margin, in *The Geology of Alaska*, edited by G. Plafker and H. C. Berg, *The Geology of North America, G–1*, 389–449, Geol. Soc. of Am., Boulder, Colo.

Plafker, G., G. Carver, L. Cluff, and M. Metz (2006), Historic and paleoseismic evidence for non-characteristic earthquakes and the seismic cycle at the Delta River crossing of the Denali fault, Alaska, *Geol. Soc. Am. Abstr. Programs, 38*, 96.

Power, M. A. (1988), Microearthquake seismicity on the Duke river, Denali fault system: Yukon, *Geology, 2*, 61–68.

Richter, D., and N. Matson (1971), Quaternary faulting in the eastern Alaska Range, *Geol. Soc. Am. Bull., 82*, 1529–1539.

Ridgway, K. D. (1992), Cenozoic tectonics of the Denali fault system, Saint Elias Mountains, Yukon Territory: Synorogenic sedimentation, basin development, and deformation along a transform fault system, Ph.D. thesis, University of Rochester, Rochester, NY.

Ridgway, K. D., and P. G. DeCelles (1993a), Stream-dominated alluvial-fan and lacustrine depositional systems in Cenozoic strike-slip basins, Denali fault system, Yukon Territory, Canada, *Sedimentology, 40*, 645–666.

Ridgway, K. D., and P. G. DeCelles (1993b), Petrology of Mid-Cenozoic strike-slip basins in an accretionary orogen, St. Elias Mountains, Yukon Territory, Canada, in *Processes Controlling the Composition of Clastic Sediments*, edited by M. J. Johnson and A. Basu, *Geol. Soc. Am. Spec. Pap. 284*, 67–89.

Ridgway, K. D., T. Skulski, and A. R. Sweet (1992), Cenozoic displacement along the Denali fault system, Yukon Territory: Abstracts with Programs, *Eos Trans. AGU, 73,* Fall Meeting Suppl., 534.

Ridgway, K. D., A. R. Sweet, and A. R. Cameron (1995), Climatically induced floristic changes across the Eocene–Oligocene transition in the northern high latitudes, Yukon Territory, Canada, *Geol. Soc. Am. Bull., 107*, 676–696.

Ridgway, K. D., J. M. Trop, and A. R. Sweet (1999), Stratigraphy, depositional systems, and age of the Tertiary White Mountain basin, Denali fault system, southwestern Alaska, *Short Notes Alaska Geol., 119*, 77–84.

Ridgway, K. D., J. M. Trop, W. J. Nokleberg, C. M. Davidson, and K. R. Eastham (2002), Mesozoic and Cenozoic tectonics of the eastern and central Alaska Range: Progressive basin development and deformation in a suture zone, *Geol. Soc. Am. Bull., 114*, 1480–1504.

Sheaf, M. A., L. Serpa, and T. L. Pavlis (2003), Exhumation rates in the St. Elias Mountains, Alaska, *Tectonophysics, 367*, doi:10.1016/soo40-1951(03)00124-0.

Skulski, T., D. Francis, and J. Ludden (1991), Arc-transform magmatism in the Wrangell volcanic belt, *Geology, 19*, 11–14.

Skulski, T., D. Francis, and J. Ludden (1992), Volcanism in an arc-transform transition zone: The stratigraphy of the St. Clare Creek volcanic field, Wrangell volcanic belt, Yukon, Canada, *Can. J. Earth Sci., 29*, 446–461.

St. Amand, P. (1957), Geological and geophysical synthesis of the tectonics of portions of British Columbia, the Yukon Territory, and Alaska, *Geol. Soc. Am. Bull., 68*, 1343–1370.

Stout, J. H., and C. G. Chase (1980), Plate kinematics of the Denali fault system, *Can. J. Earth Sci., 17*, 1527–1537.

Trop, J. M., and K. D. Ridgway (2007), Mesozoic and Cenozoic sedimentary basin development along the inboard and outboard margins of the Wrangellia composite terrane, in *Tectonic Growth of a Collisional Continental Margin: Crustal Evolution of Southern Alaska*, edited by K. D. Ridgway et al., *Geol. Soc. Am. Spec. Pap. 431*, 55–94, doi:10.1130/2007.2431(04).

Trop, J. M., K. D. Ridgway, and A. R. Sweet (2004), Stratigraphy, palynology, and provenance of the Colorado Creek basin: Oligocene transpressional tectonics along the central Denali fault system, *Can. J. Earth Sci., 41*, 457–480.

Worrall, D. M. (1991), Tectonic history of the Bering Sea and the evolution of Tertiary strike-slip basins of the Bering Shelf, *Geol. Soc. Am. Spec. Pap. 257*, 120 pp.

Wright, F. E., and C. W. Wright (1908), Ketchikan and Wrangell mining districts, *U.S. Geol. Surv. Bull., 347*, 210 pp.

_____

A. M. Freed, J. L. Kalbas, and K. D. Ridgway Department of Earth and Atmospheric Sciences, Purdue University, 550 Stadium Mall Drive, West Lafayette, IN 47907-2051, USA. (jay.l.kalbas@exxonmobil.com)